



Optimized deposition and characterization of nanocrystalline magnesium indium oxide thin films for opto-electronic applications

A. Moses Ezhil Raj^a, C. Ravidhas^b, R. Ravishankar^c, A. Rathish Kumar^c, G. Selvan^e,
M. Jayachandran^c, C. Sanjeeviraja^{d,*}

^a Departments of Physics, Scott Christian College (Autonomous), Nagercoil 629 003, India

^b Department of Physics, Bishop Heber College (Autonomous), Tiruchirapalli 620 017, India

^c Central Electrochemical Research Institute, Karaikudi 630 006, India

^d Department of Physics, Alagappa University, Karaikudi 630 003, India

^e Department of Physics, Thanthai Hans Roever College, Perambalur 621 212, India

ARTICLE INFO

Article history:

Received 4 May 2008

Received in revised form 30 August 2008

Accepted 24 October 2008

Available online 11 November 2008

PACS:

68.55._a

81.20.Ka

61.05.cp

68.37.Ps

73.50._h

Keywords:

A. Thin films

B. Chemical synthesis

C. X-ray diffraction

C. Atomic force microscopy

D. Electrical properties

ABSTRACT

Transparent conducting magnesium indium oxide films (MgIn_2O_4) were deposited on to quartz substrates without a buffer layer at an optimized deposition temperature of 450 °C to achieve high transmittance in the visible spectral range and electrical conductivity in the low temperature region. Magnesium ions are distributed over the tetrahedral and octahedral sites of the inverted spinel structure with preferential orientation along (3 1 1) Miller plane. The possible mechanism that promotes conductivity in this system is the charge transfer between the resident divalent (Mg^{2+}) and trivalent (In^{3+}) cations in addition to the available oxygen vacancies in the lattice. A room temperature electrical conductivity of $1.5 \times 10^{-5} \text{ S cm}^{-1}$ and an average transmittance >75% have been achieved. Hall measurements showed n-type conductivity with electron mobility value $0.95 \times 10^{-2} \text{ cm}^2 \text{ V}^{-1} \text{ s}^{-1}$ and carrier concentration $2.7 \times 10^{19} \text{ cm}^{-3}$. Smoothness of the film surface observed through atomic force microscope measurements favors this material for gas sensing and opto-electronic device development.

Crown Copyright © 2008 Published by Elsevier Ltd. All rights reserved.

1. Introduction

Transparent conducting oxides (TCOs) are materials of both fundamental interest and technological importance due to the possibility of synthesizing them in the form of nanowires, nanoneedles and nanotubes [1,2]. Basically, TCOs are insulators in their stoichiometric form, whereas in non-stoichiometric form they behave as highly conducting semiconductors with wide direct band gap ($E_g > 3 \text{ eV}$) and possess high optical transmittance [3]. In addition, electrical conductivity is found originated from the charge transfer between the cations and also from the oxygen vacancies created on adding dopant to the crystal matrix. Although the optical and electrical properties tend to eliminate each other, TCO materials have both electrical conduction ($\approx 10^4 \text{ S cm}^{-1}$) and

optical transparency (>90%) in the visible region [4]. Some important semiconductors of this kind are the post transition binary metallic oxides, such as ZnO, SnO_2 , Ga_2O_3 , In_2O_3 and CdO nanocrystalline thin films containing nanobelts/nanowires/nanoparticles [5–7]. These films find widespread applications: as transparent electrodes in opto-electronic devices like light emitting diodes, flat-panel displays, photovoltaic/photo-electrochemical solar cells [8,9], as heat-reflecting coatings on architectural windows, gas sensors [10,11], defogging coatings in aircraft and automobile windows and wear resistance layers on glass [12,13].

Among the many applications, it is observed that low cost gas sensors for sensing inflammable gases can be realized by using binary SnO_2 , In_2O_3 and ZnO semiconductors [14,15]. However the devices fabricated using these materials consume large power consumption and the sensitivity strongly depends on their physical and chemical properties. It is very difficult to modify the physical and chemical properties of binary materials and therefore

* Corresponding author.

E-mail address: sanjeeviraja@rediffmail.com (C. Sanjeeviraja).

recently tailoring the physico-chemical properties of metal oxide thin films have been realized by engaging new semiconductor materials consisting of multicomponent oxides according to the proposed hypothesis [16]. Based on this working hypothesis, potential transparent conducting oxides like; MgIn_2O_4 [17,18], $\text{Zn}_x\text{Mg}_{(1-x)}\text{O}$ [19], CdIn_2O_4 [20,21], CdGa_2O_4 [22], ZnGa_2O_4 [23], Zn_2SnO_4 [24] and Cd_2SnO_4 [25] have been studied recently. Among these ternary oxides, MgIn_2O_4 thin film finds application as a new transparent as well as active electrode in photo-electrochemical solar cells [26] and as sensing element in gas sensors [27–30]. In addition, it exhibits a number of superior properties such as low resistivity, high adhesion, thermal stability, low absorbance in the visible spectral region, and more compatible to have smooth interface.

MgIn_2O_4 is an n-type wide-band gap semiconductor (>3 eV), which has a separate conducting path in the crystal lattice. It has the general spinel structure based on a cubic close packed array of anions with the formula AB_2O_4 , where A and B are generally either divalent and trivalent metal ions, respectively (the so-called 2,3 spinels) or tetravalent and divalent (the 4,2 spinels). However, MgIn_2O_4 falls under inverse spinel category, according to the lattice substitution of Mg^{2+} and In^{3+} cations in the tetrahedral and octahedral voids in the fcc-cp oxygen sub-lattice. The crystallographic parameters needed to define the structure (in the space group $\text{Fd}\bar{3}\text{m}$, cubic) are the cell parameter, a and the oxygen (anion) parameter u . Essentially, u describes the deviation of the anion sub-lattice from regular close-packing, and will obviously vary according to the relative sizes of the cations in the structure [16].

There are limited numbers of deposition techniques that have been employed for the preparation of MgIn_2O_4 thin films like pulsed laser deposition [31], combustion synthesis [32] and magnetron sputtering [33]. Present study deals with the deposition of MgIn_2O_4 films using chemical spray pyrolysis (CSP) technique. Simplicity and economic viability are the attractive factors in forming thin films using this CSP deposition technique. In addition, it has certain advantages such as high deposition rate and the possibility to coat large areas with non-planar geometries where the solution is atomized onto a heated substrate placed inside a tubular furnace. During flight through the heated tubular column, fine droplets undergo evaporation, condensation, drying, thermolysis, vaporization and finally film is formed on the heated substrate by heterogeneous reactions. These aspects have been investigated for the improvement of the yield process, film structure and microstructure by optimizing the deposition parameters such as carrier gas flow, precursor concentration and deposition temperature [34]. The novelty of the present paper lies in optimizing the deposition conditions to obtain monophasic multicomponent MgIn_2O_4 thin films with nanograins useful for the fabrication of gas sensors and the results are presented.

2. Experimental

Magnesium indium oxide thin films were prepared in an indigenously built chemical spray pyrolysis set-up capable of heating up to 1000°C . The spray pyrolysis set-up and the detailed procedure adopted for the deposition of thin films have been described elsewhere [35]. The precursor solutions were prepared by dissolving magnesium acetate [$\text{Mg}(\text{CH}_3\text{COO})_2 \cdot 4\text{H}_2\text{O}$] and indium chloride (InCl_3) in 100% ethanol for the cationic ratio $\text{Mg}/\text{In} = 0.5$. A small amount of concentrated hydrochloric acid was used to dissolve the salts without any precipitation, to make the solution clear and also for stabilization. Films were deposited on quartz substrates at three different temperatures 400, 450 and

Table 1

Optimized preparative parameters for synthesis of MgIn_2O_4 thin films.

No.	Preparative parameters	Optimized values
1	Precursor solute	$\text{Mg}(\text{CH}_3\text{COO})_2 \cdot 4\text{H}_2\text{O} + \text{InCl}_3$
2	Precursor concentration	0.1 M
3	Precursor solvent	100% ethanol
4	Cationic ratio (Mg/In)	0.5
5	Substrate temperature	450°C
6	Spray rate	5 ml/min
7	Solution quantity	25 ml
8	Carrier gas pressure	0.4 kg/cm^2
9	Substrate-nozzle distance	30 cm

500°C by spraying 25 ml of the precursor. These deposition temperatures were chosen only after getting prior knowledge about the decomposition behavior of the precursors, magnesium acetate and indium chloride, to their respective oxides. The required deposition parameters to obtain high quality films were optimized by controlling the associated process parameters listed in Table 1. Polycrystalline powder sample of MgIn_2O_4 was also synthesized from MgCO_3 and In_2O_3 powders. In the present investigations, to have stoichiometry, one mole of magnesium carbonate and two moles of indium oxide powders were mixed and were calcined at 600°C for 24 h followed by sintering at 1000°C for 48 h. The sintered powder was tested by XRD analysis and formation of single phase MgIn_2O_4 was confirmed.

The MgIn_2O_4 films deposited under the optimized preparative conditions are transparent, well adherent to the substrate and are very smooth. However, on exposing the film to ambient atmosphere, the process of adsorption of water in to the crystal lattice takes place, which is normally common in the case of spray deposited films. Films prepared under identical conditions have thickness values in the range of $0.35\text{--}0.40 \mu\text{m}$ as estimated by the Stylus profilometer (Mitutoyo). Moreover, the stability of the film has a strong dependence on the critical size of the nucleus of the atomic species. Stability increases with size, making dissociation and re-evaporation extremely unlikely as in the case of magnesium and indium. Quartz substrate also has low surface energy than the surface energy of the condensate material, which enhances the critical size of the clusters and increases the stability and smoothness of the film. Surface smoothness and morphology of the deposited films were investigated using atomic force microscope (Nanoscope-E AFM/STM). XRD spectra were recorded with a PANalytical-3040 X'pert Pro diffractometer with $\text{Cu K}\alpha$ radiation of wavelength 1.5406 \AA ($\theta\text{--}2\theta$ scan) in the scanning range of 10° to 80° (2θ). The sample was rotated while the scan was recorded. All the peaks in the diffraction pattern were indexed on the basis of a Joint Committee for Powder Diffraction Studies (JCPDS) data. The metal-oxygen bonding and vibrational modes were investigated from the Fourier transform infrared (FTIR) spectra recorded in Thermo Nicolet Nexus spectrometer. The FTIR spectra were recorded in the wave number range of $400\text{--}4000 \text{ cm}^{-1}$, with a spectral resolution of 1 cm^{-1} . The elemental composition of the film was analyzed using energy dispersive X-ray (EDX) spectrometer attached with the HITACHI S-3000H SEM instrument. The sheet resistance and conductivity were measured using the conventional four-probe method in the temperature range $30\text{--}150^\circ\text{C}$. The effective carrier concentration and mobility were calculated using Hall probe measurements. For electrical measurements, ohmic contacts were provided by sputtering Ag metal and were contacted by Cu wires. Optical transmittance measurements were recorded using a Hitachi-330 UV-vis-NIR spectrophotometer in the wavelength range of $280\text{--}1500 \text{ nm}$.

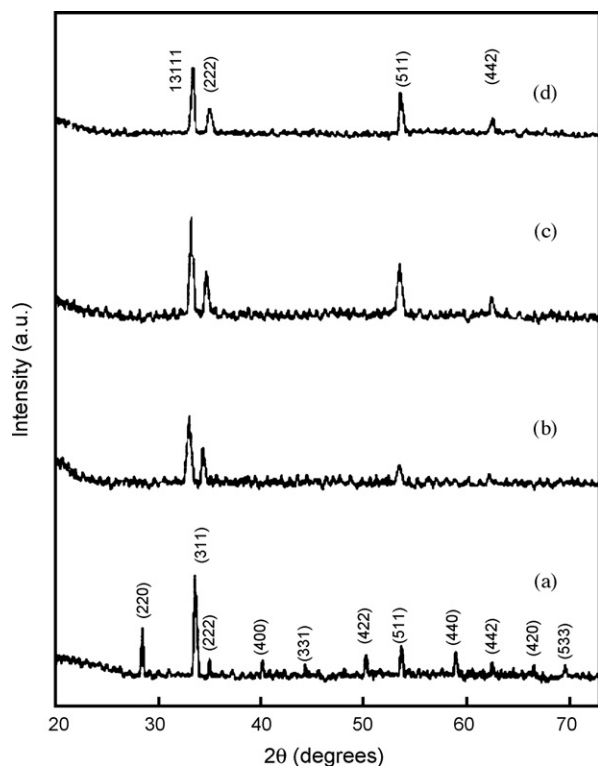


Fig. 1. XRD patterns of MgIn_2O_4 : (a) synthesized by the calcination process, (b) prepared by spray pyrolysis at 400 °C, (c) 450 °C and (d) 500 °C.

3. Results

The XRD spectra of the MgIn_2O_4 films prepared at 400, 450 and 500 °C for the cation stoichiometry ratio 1:2 (Mg:In) and for the calcined MgIn_2O_4 powder sample is shown in Fig. 1. At these deposition temperatures, the thermal decomposition of the precursor is completed that leads to polycrystalline and single phase spinel oxide. The dimension of the grains and other related parameters were estimated from the (3 1 1) crystal plane, which exhibits the maximum intensity. However, the powder sample has almost all the peaks, indexed according to the standard data. The optimum growth temperature for MgIn_2O_4 thin film was found to be 450 °C at the carrier gas pressure of 0.4 kg/cm².

The completeness of the precursor decomposition is indicated in the FTIR spectra by the presence of the sharp bands in the visible

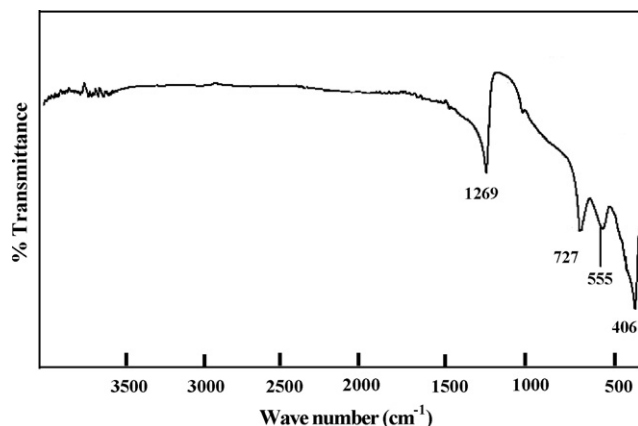


Fig. 2. FTIR spectrum of the sprayed MgIn_2O_4 film at 450 °C.

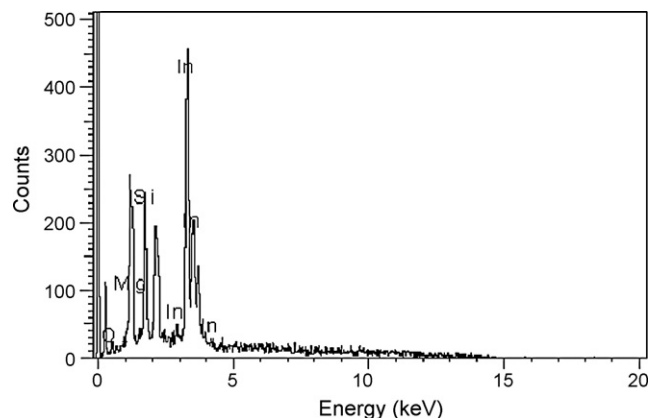


Fig. 3. EDAX spectrum of the MgIn_2O_4 film deposited at 450 °C.

and near-infrared region which are associated with the longitudinal optical phonon modes for the metal-oxide stretching (Fig. 2). Adsorbed water molecules reveal bands corresponding to 1276 and 727 cm^{-1} . The MgIn_2O_4 phase formation is further confirmed with the elemental analysis through the energy dispersive X-ray absorption spectrum (Fig. 3). The microanalysis spectrum reveals respective peaks only for magnesium, indium and oxygen without any contaminations including chlorine.

Fig. 4 shows the temperature-dependent electrical conductivity of the MgIn_2O_4 films deposited at 450 °C. The room temperature conductivity of the film is $1.5 \times 10^{-5} \text{ S cm}^{-1}$, whereas $1.24 \times 10^{-4} \text{ S cm}^{-1}$ is observed at 150 °C. Degenerate semiconducting behavior is observed from the conductivity variations. The optical property of magnesium indium oxide films are characterized from the optical transmittance data (Fig. 5). About 75% transmittance is observed in the visible region, whereas in the IR region optical transmittance is more than 80%. The absorption coefficient values are found to be in the order of 10^4 cm^{-1} .

The AFM image of the magnesium indium oxide film shown in Fig. 6 clearly indicates the columnar growth structure with nearly the same shape and size. The Grains have perfect flat surface when it is viewed over a single grain located in a line lying between the points (1156.3 and 476.6 nm) and (1312.5 and 476.6 nm) as shown in Fig. 6c. The surface roughness of 2.2 nm is measured from the surface scan (Fig. 7).

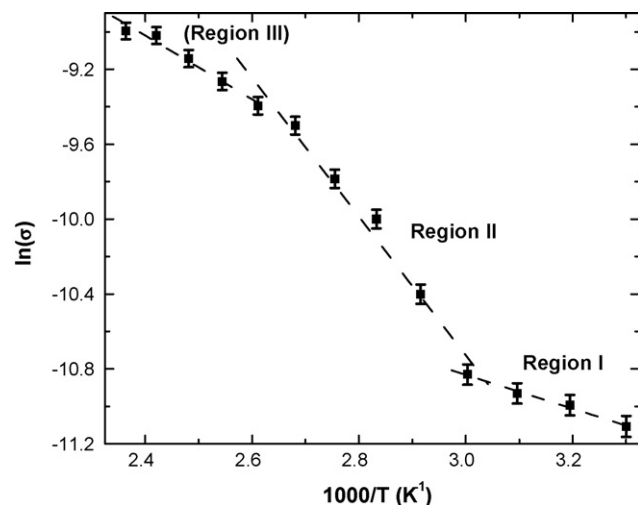


Fig. 4. Arrhenius plot drawn from the conductivity measurement of the MgIn_2O_4 film.

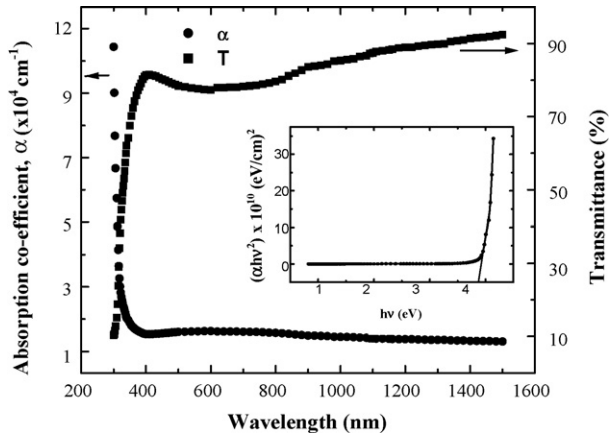
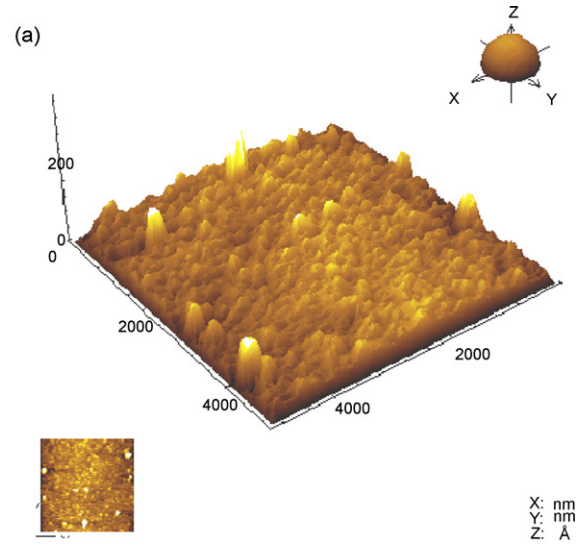


Fig. 5. Optical absorption co-efficient and transmittance spectrum of MgIn₂O₄ film. Inset is the Tauc plot for estimating the optical band gap.



4. Discussion

The formation of single phase MgIn₂O₄ films at different substrate temperatures was confirmed from the recorded X-ray diffraction spectra (Fig. 1). The powder sample has almost all the peaks indexed according to the standard data (JCPDS card no.: 73-2414) [36]. Thin film samples exhibit polycrystalline nature and have preferential orientation along (3 1 1) plane. No characteristic peaks of impurity/dopant phases are seen. However, the diffraction peaks of the film deposited at 450 °C are the strongest. It demonstrates that the grains of the film prepared at this temperature would crystallize more perfectly and possess better crystallinity. Moreover, the wider peaks indicate that the films are composed of small nanocrystallites. Films prepared at 400 and 500 °C are also crystalline, but the peak intensities are less which mainly depends on the substrate temperature. At 400 °C, the available thermal energy is not sufficient to form dense MgIn₂O₄ film as confirmed from the observed density value of 6.014 gm/cm³ which is less compared to the bulk value. The film deposited at 500 °C is denser than the film prepared at 450 °C, but the thickness of the film is less due the re-evaporation of precursor that induces heterogeneous reaction well above the substrate surface. Consequently, the final MgIn₂O₄ product is formed in less quantity which in turn gives XRD peaks with less intensity as revealed from the recorded XRD spectrum. In addition, the variation in the density of the films with substrate temperature is also confirmed from the observed shift of the peaks to lower diffraction angles. These observations are similar to the reported results on indium oxide powder heat treated at different temperatures [37].

The lattice constant *a* was calculated from the intense peak emerged from the lattice plane indexed (3 1 1) using the formula:

$$\frac{1}{d_{hkl}^2} = \frac{h^2 + k^2 + l^2}{a^2} \tag{1}$$

The unit cell dimension of the films deposited at 450 °C was found to be 8.884 Å, which is comparable to the standard bulk value 8.864 Å [36]. The full width at half maximum of the (3 1 1) diffraction peak was used to estimate the crystallite dimension using Scherrer's equation:

$$D = \frac{k\lambda}{\sqrt{(\beta^2 - \beta_0^2)} \cos \theta} \tag{2}$$

where *D* is the crystallite size, *k* is a constant (0.94), λ is the wavelength of X-ray (1.5406 Å for the Cu K α line), β is the full width at half maximum (FWHM) of the respective peak, β_0 is the

Fig. 6. AFM micrographs of the MgIn₂O₄ films deposited at optimized conditions: (a) large area 3D scan, (b) small area 2D scan and (c) single grain scan.

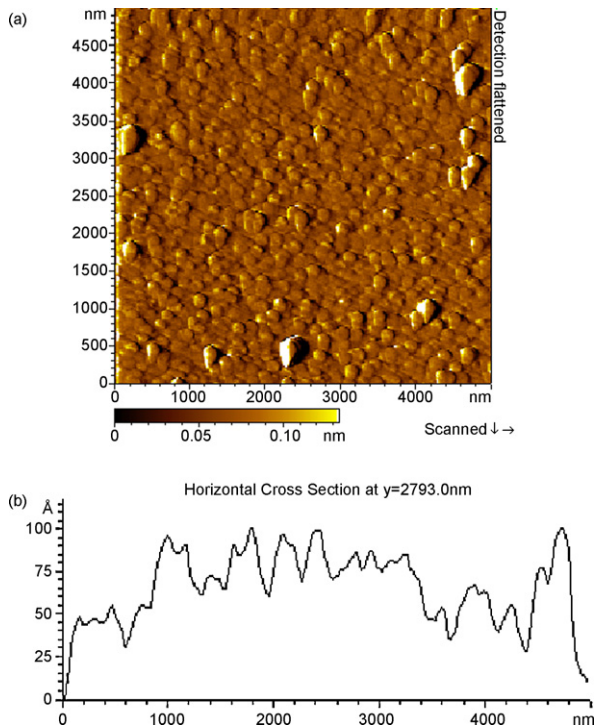


Fig. 7. (a) AFM image in 2D and (b) surface roughness profile of the MgIn_2O_4 film.

integral peak width caused by instrumental broadening and θ is the corresponding Bragg's angle. The crystallite size was found to be about 52 nm for the films deposited at 450 °C.

The origin of the strain is also related to the lattice mismatch and may be calculated from the slope of $\beta \cos \theta$ vs. $\sin \theta$ plot using the relation:

$$\varepsilon = \frac{\lambda}{D \sin \theta} - \frac{\beta}{\tan \theta} \quad (3)$$

The microstrain of the optimized film was positive and was estimated equal to 6.2×10^{-4} , which was comparatively less than that of the film deposited at 400 and 500 °C. An explicit inverse correlation between the estimated size and microstrain was also observed.

The dislocation density δ , which is the number of dislocation lines per unit area of the crystal was also evaluated from the crystallite size D using the formula:

$$\delta = \frac{1}{D^2} \text{ lines/m}^2 \quad (4)$$

Dislocation density of the film prepared at 450 °C was observed to be about 3.73×10^{14} lines/m². At the optimized deposition condition, both the microstrain and dislocation density of the MgIn_2O_4 films are minimum revealing substantial reduction in the concentration of lattice imperfections. This might have made the grains to arrange themselves in a preferentially oriented manner [38].

Using crystallite size D and film thickness t , number of crystallites N has been estimated using the relation:

$$N = \frac{t}{D^3} / \text{unit area} \quad (5)$$

and the number of crystallites estimated was nearly $2.88 \times 10^{15}/\text{m}^2$.

If the unit cell of volume V (\AA^3) contains Z formula units, the density of the deposited films can be calculated using the formula:

$$\rho = \frac{\text{formula weight} \times Z \times 1.66}{V} \quad (6)$$

For inverse spinels like MgIn_2O_4 , oxygen ions occupy fcc packing with the cations occupying one eighth of the tetrahedral sites and one-half of the octahedral sites. The ions are arranged such that each unit cell consists of eight oxygen cubes and therefore the unit cell contents have eight formula units ($Z = 8$). The calculated density value of 6.023 g/cm^3 is comparable with the standard bulk value 6.065 g/cm^3 . It shows that spray pyrolysis technique is capable of producing stoichiometric MgIn_2O_4 films possessing similar properties as that of the bulk material.

The IR transmission spectrum of the MgIn_2O_4 films recorded in the wave number range $400\text{--}4000 \text{ cm}^{-1}$ is shown in Fig. 2. The weak peak at 1276 cm^{-1} is assigned to the water bending vibrations. An out-of-plane bending mode of water is also seen at 727 cm^{-1} [39]. These bands reveal the presence of water of hydration which is normally incorporated into the lattice of oxide films due to the adsorption of water molecules when it was exposed to atmosphere [40]. Further there is no sign of absorption band arising from free carrier absorption and is compromised only partially by charge-transfer absorption at shorter wavelengths and a few sharp bands from vibrations of the oxygen lattice between 400 and 650 cm^{-1} [41,42]. The two absorption peaks at 555 and 406 cm^{-1} observed in the finger print region, are associated with the longitudinal optical phonon modes for the metal-oxide stretching in the octahedral sites [43]. This implies that the film mainly consists of MgIn_2O_4 with less amount of water of crystallization.

These observations are further confirmed from the results of elemental analysis through the energy dispersive X-ray absorption spectrum (Fig. 3). The microanalysis spectrum reveals the presence of respective peak for magnesium, indium and oxygen without any contaminations including chlorine which is normally noticeable in spray pyrolysis coatings. The atomic percentage of magnesium, indium and oxygen present in the deposited films were calculated from the peak intensities and the area under the peak of the corresponding elements. The atomic percentage of magnesium is 31.26%, whereas for indium 68.74% is observed. The Mg/In atomic ratio of 0.46 thus obtained is comparable to the value of 0.5 in the precursor which reveals the purity of the deposited MgIn_2O_4 films.

Conductivity measurements were carried out in the temperature range between 30 and 150 °C by the four-probe technique. Fig. 4 shows the temperature-dependent electrical conductivity of the MgIn_2O_4 films deposited at 450 °C. It reveals three distinct regions having different slopes, corresponding to low temperature (region-I), intermediate temperature region (region-II) and high temperature (region-III) region. In region-I, the conductivity is almost constant up to 67 °C after that it increases rapidly with increasing temperature up to 130 °C. Again, the conductivity of the sample remains almost constant above 130 °C. The increase in conductivity of the samples with temperature may be due to decrement in grain boundary concentration and increase in oxygen vacancies [44], which enhances the carrier concentration and mobility of the charge carriers. It was also observed that the steep fall in resistance during the time of first heating was comparatively large than that observed in successive heating. During first time heating, resistivity decreases due to scattering of the charge carriers by the distributed point defects in the crystal lattice. On heating the film, the rearrangements and elimination of point defect clusters leads to an increase in carrier concentration. Repeated heating of the same sample alters the variations and therefore error bars are introduced in the conductivity plot. The

room temperature conductivity of the film is $1.5 \times 10^{-5} \text{ S cm}^{-1}$, whereas $1.24 \times 10^{-4} \text{ S cm}^{-1}$ is observed at 150°C . Their temperature-dependent conductivity reveals the degenerate semiconducting nature of the deposited MgIn_2O_4 films due to small variations in electrical conductivity.

The measured conductivity may be fitted with the following expression:

$$\sigma = \sigma_0 \exp\left(-\frac{E_a}{kT}\right) \quad (7)$$

where σ_0 is the pre-exponent factor, k is Boltzmann constant, T is the temperature and E_a is the activation energy.

From the slope of the fitted curve, the activation energy was calculated in all the three regions and is listed in Table 2. The activation energy value in region-I indicates the presence of a shallow donor levels near the bottom of the conduction band, where as the activation energy in region-II indicates the presence of deep donor levels. So in region-I, there is prevalence of extrinsic conduction and in region-II there is intrinsic conduction domain. In region-III, the charge carriers available for conduction is saturated and therefore the resistivity variation is not abrupt and the activation energy is still low (0.14 eV).

Hall probe measurement shows that the carriers are electrons (n-type) that are generated from interstitials or from substituted cations and/or from oxygen vacancies. The carrier concentration is found to be $2.7 \times 10^{19} \text{ cm}^{-3}$. Even though the carrier concentration is high, the as-deposited MgIn_2O_4 film has low electrical conductivity of about $1.5 \times 10^{-5} \text{ S cm}^{-1}$ at RT. The overall lower conductivity is attributed to the stoichiometric nature of the film which shows higher crystallinity with very low carrier mobility values in the range of $10^{-2} \text{ cm}^2 \text{ V}^{-1} \text{ s}^{-1}$. Such a relatively low electron mobility for the MgIn_2O_4 films may be arising due to the disorder on the cation octahedral sites which disrupt carrier transport between edge-sharing $d^{10}s^0$ electronically configured cations.

The optical transmittance spectrum of spray deposited MgIn_2O_4 films prepared on quartz substrates at 450°C is shown in Fig. 5. It is observed that the transmittance value increases with the increase of wavelength. About 75% transmittance is observed in the visible region, whereas in the IR region optical transmittance is more than 80%. This value of transmittance is well agreement with the previously reported values for the MgIn_2O_4 films prepared in other deposition techniques [17,31].

The absorption co-efficient α of the optimized film was calculated from the transmittance spectrum using the relation:

$$\alpha = \frac{2.303[\log(1/T)]}{t} \quad (8)$$

where T is the optical transmittance. The absorption co-efficient is found to be about 10^4 cm^{-1} , which exponentially decreases as photon energy decreases. In order to confirm the nature of optical

Table 2
Electrical and optical data of the MgIn_2O_4 film.

No.	Parameters	Values
1	Conductivity (S cm^{-1})	1.24×10^{-4} – 1.5×10^{-5}
2	Activation energy (eV)	0.34 (Region-I) 0.57 (Region-II) 0.14 (Region-III)
3	Carrier concentration (cm^{-3})	2.7×10^{19}
4	Mobility ($\text{cm}^2 \text{ V}^{-1} \text{ s}^{-1}$)	0.95×10^{-2}
5	Transmittance (%)	>75
6	Optical band gap (eV)	3.82

transition in the prepared films, the optical data were analyzed using the equation:

$$\alpha h\nu = \alpha_0(h\nu - E_g)^n \quad (9)$$

where E_g is the separation between bottom of conduction band and top of the valence band, α_0 is a constant, $h\nu$ is the photon energy, and n is a constant.

For allowed direct transition $n = 1/2$ and for allowed indirect transition $n = 2$. The plots of $(\alpha h\nu)^2$ against $h\nu$ for the magnesium indium oxide films deposited at 450°C is shown in Fig. 5. The nature of the plots suggests an direct interband transition. The straight line region is extrapolated to $\alpha = 0$ and the energy-axis intercept is considered to be the optical band gap value (E_g). The optical band gap energy of MgIn_2O_4 is found to be 3.82 eV, which is greater than that of MgIn_2O_4 sputtered films [17]. Usually, spinel thin films are having transmittance in the range 80–90%, which is quite common and exhibit fundamental absorption edge at about 340 nm [45]. The increased band gap value may be attributed to the smaller crystalline size which makes the spray deposited MgIn_2O_4 film a novel transparent and conducting oxide material for opto-electronic devices and gas sensors.

The AFM morphology displays a granular structure with spherical-shaped grains of dimensions ranging from about 95 to 112 nm. Fig. 6c shows the scan of a typical single grain marked in Fig. 6b at the location (1156.3–1312.5 and 476.6 nm), whose size is in nanoscale of about 98 nm. The quantitative analysis of the surface roughness is carried out on large scale images, by using the root mean square [RMS (R_q)] function software of the Nanoscope III-DI. Standard deviation of the surface height (R_{p-v}), average roughness (R_a) and RMS roughness calculations were performed at all points on the roughness profile obtained by scanning the 2D images along the diagonal line of the surface shown in Fig. 7a. It shows the 2D AFM image of the MgIn_2O_4 surface scanned over an area of $5.0 \mu\text{m} \times 5.0 \mu\text{m}$ which is essentially homogeneous. Fig. 7b shows the surface roughness profile obtained by scanning this surface along the line marked at 2793 nm. The observed maximum peak to valley roughness R_{p-v} is 35 nm and the average roughness R_a is 1.6 nm.

The root mean square (RMS) roughness of the film surface is calculated using the least-square fitted line of the surface profile (Fig. 7b) which is expressed by the following equation,

$$\text{RMS roughness} = \left[\frac{1}{N_L} \sum_{i=1}^{N_L} Z_i^2(x) \right]^{1/2} \quad (11)$$

where N_L is the number of discrete measurement points on the profile and $Z(x)$ is the height deviation of the profile from a least-square fitted line. The RMS roughness of the MgIn_2O_4 film is 2.2 nm which shows that the surface is smooth enough to transmit light for transparent coating and sensor applications.

The film sensitivity correlation with surface parameters can be explained using the conduction model of metal oxide gas sensors approximation given by Barsan and Weimar [46]. The principle of gas detection is the interaction of gaseous species with the surface of the semiconducting oxide layer. At the time of interaction, charge transfer takes place between the absorbed species and the semiconductor sensor [47]. The model explains that the surface influence on the mobility becomes dominant over bulk phenomena when the mean free paths of the charge carriers are equal to grains of smaller size. In the presence of the ionic species on the surface, the electronic concentration in the surface states increases. The surface states concentration is correlated with the roughness and grain size via surface-to-volume ratio. Therefore, the gas sensitivity is directly proportional to the film roughness

which proves the importance of surface-to-volume ratio for developing highly sensitive sensors.

5. Conclusions

Chemically stable and highly crystalline MgIn_2O_4 films have been prepared using spray pyrolysis deposition technique on quartz substrates. The XRD studies revealed the cubic structure with a lattice constant of 8.884 Å which is very close to the standard value. The infrared spectrum is reasonably transparent and no absorption bands arising from free carrier absorption or reflection are seen. The atomic ratio of magnesium and indium in the film is 0.46 which is nearly the same as present in the precursor ($\text{Mg/In} = 0.5$). The temperature-dependent electrical conductivity has three regions with different activation energies in the temperature range 30–150 °C. The observed very low electrical conductivity values (10^{-5} to $10^{-4} \text{ S cm}^{-1}$) is mainly due to the polaron type conduction which drastically decreased the carrier mobility value. Stoichiometric MgIn_2O_4 film shows an absorption edge at 310 nm corresponding to an optical band gap of 3.82 eV. AFM image shows a pore-free morphology with spherical grains of uniform size distributed all over the surface. From the observed electrical, optical and surface morphological properties, it can be concluded that the magnesium indium oxide films fabricated by the chemical spray pyrolysis technique under the optimized conditions are suitable for opto-electronic applications. Electrical conductivity can be improved by implanting lighter ions into the crystal lattice and the work is now in progress.

References

- [1] J.G. Lu, P. Chang, Z. Fan, *Mater. Sci. Eng. R: Rep.* 52 (2006) 49.
- [2] N.V. Hieu, H.R. Kim, B.K. Ju, J.H. Lee, *Sens. Actuators B: Chem.* 133 (2008) 228.
- [3] A. Antony, M. Nisha, R. Manoj, M.K. Jayaraj, *Appl. Surf. Sci.* 225 (2004) 294.
- [4] C.P. Udawatte, K. Yanagisawa, *J. Solid State Chem.* 154 (2000) 444.
- [5] W.P. Zhang, R.D. Zu, L.W. Zhang, *Science* 291 (2001) 1947.
- [6] Z. Li, B. Zhao, P. Liu, Y. Zhang, *Microelect. Eng.* 85 (2008) 1613.
- [7] H.W. Kim, S.H. Shim, *Chem. Phys. Lett.* 422 (2006) 165.
- [8] H. Klauk, *Nature* 451 (2008) 533.
- [9] D.I. Suh, S.Y. Lee, T.H. Kim, J.M. Chun, E. Ksuh, O.B. Yang, S.K. Lee, *Chem. Phys. Lett.* 442 (2007) 348.
- [10] T.J. Hsueh, C.H. Hsu, S.J. Chang, I.C. Chen, *Sens. Actuators B: Chem.* 126 (2007) 473.
- [11] A. Vomiero, S. Binachi, E. Comini, G. Faglia, M. Ferroni, N. Poli, G. Sberveglieri, *Thin Solid Films* 515 (2007) 8356.
- [12] N.G. Patel, P.D. Patel, V.S. Vaishnav, *Sens. Actuators B: Chem.* 96 (2003) 180.
- [13] F. Zhu, K. Zhang, E. Guenther, C.S. Jin, *Thin Solid Films* 363 (2000) 314.
- [14] S. Chakraborty, A. Sen, H.S. Maiti, *Sens. Actuators B* 119 (2006) 431.
- [15] G. Korotcenkov, M. Ivanov, I. Blinov, J.R. Stetter, *Thin Solid Films* 515 (2007) 3987.
- [16] H. Kawazoe, N. Ueda, H. Un'no, T. Omata, H. Hosono, H. Tanoue, *J. Appl. Phys.* 76 (1994) 7935.
- [17] T. Minami, S. Takata, T. Kakumu, H. Sonohara, *Thin Solid Films* 270 (1995) 22.
- [18] D. Bacorisen, R. Smith, J.A. Ball, R.W. Grimes, B.P. Uberuaga, K.E. Sickafus, W.T. Rankin, *Nucl. Instrum. Methods Phys. Res. B* 250 (2006) 36.
- [19] H.W. Kim, J.W. Lee, S.H. Shim, *J. Phys. Chem. Solids* 69 (2008) 1491.
- [20] P. Mohan Babu, G. Venkata Rao, P. Sreedhara Reddy, S. Uthanna, *Mater. Lett.* 60 (2006) 274.
- [21] H.M. Ali, H.A. Mohamed, M.M. Wakkad, M.F. Hasaneen, *Thin Solid Films* 515 (2007) 3024.
- [22] T. Omata, N. Ueda, N. Hikuma, K. Udea, H. Mizoguchi, T. Hashimoto, H. Kawazoe, *Appl. Phys. Lett.* 62 (1993) 499.
- [23] J.H. Lee, H.J. Pank, K. Yoo, B.W. Kim, J.C. Lee, S. Pank, *J. Eur. Ceram. Soc.* 27 (2007) 965.
- [24] X. Lou, X. Jia, J. Xu, S. Liu, Q. Gao, *Mater. Sci. Eng. A* 432 (2006) 221.
- [25] W.L. Wang, K.J. Liao, C.Z. Cai, G.B. Liu, Y. Ma, *Surf. Coat. Technol.* 167 (2003) 284.
- [26] P.M. Sirimanne, N. Sonoyama, T. Sakata, *J. Solid State Chem.* 154 (2000) 476.
- [27] C. Xiangfeng, J. Dongli, G. Yu, Z. Chenmou, *Sens. Actuators B* 120 (2006) 177.
- [28] T. Miyata, T. Hikosaka, T. Minami, *Sens. Actuators B* 69 (2000) 16.
- [29] A.J. Freeman, K.R. Poeppelmeier, T.O. Mason, R.P.H. Chang, T.J. Marks, *MRS Bull.* 25 (2000) 45.
- [30] J.P. Kar, M.C. Jeong, W.K. Lee, J.M. Myoung, *Mater. Sci. Eng. B* 147 (2008) 74.
- [31] A. Kudo, H. Yanagi, H. Hosono, H. Kawazoe, *Mater. Sci. Eng. B* 54 (1998) 51.
- [32] N. Ueda, T. Omata, N. Hikuma, K. Udea, H. Mizoguchi, T. Hashimoto, H. Kawazoe, *Appl. Phys. Lett.* 61 (1992) 1954.
- [33] H. Hosono, H. Un'no, N. Ueda, H. Kawazoe, N. Matsunami, H. Tanoue, *Nucl. Instrum. Methods Phys. Res. B* 106 (1995) 517.
- [34] P. Prathap, Y.P.V. Subbaiah, M. Devika, K.T. Ramakrishna Reddy, *Mat. Chem. Phys.* 100 (2006) 375.
- [35] A. Moses Ezhil Raj, L.C. Nehru, M. Jayachandran, C. Sanjeeviraja, *Cryst. Res. Technol.* 42 (2007) 867.
- [36] Joint Commission of Powder Diffraction Data Files, PCPDFWIN, Version 1.30, Pennsylvania, 1997.
- [37] S. Li, X. Qiao, J. Chen, H. Wang, F. Jia, X. Qiu, *J. Cryst. Growth* 289 (2006) 151.
- [38] A. Ashor, N. El-Kadry, M.R. Ebid, M. Farghal, A.A. Ramadan, *Thin Solid Films* 279 (1996) 242.
- [39] S. Chakrabarthy, D. Ganguli, S. Chaudhuri, *Mater. Lett.* 57 (2003) 4483.
- [40] R.K. Kwar, P.S. Chigare, P.S. Patil, *Appl. Surf. Sci.* 206 (2003) 90.
- [41] B. Lefez, P. Nkeng, J. Lopitiaux, G. Poillerat, *Mater. Res. Bull.* 31 (1996) 1263.
- [42] C.F. Windisch Jr., K.F. Ferris, G.J. Exarhos, S.K. Sharma, *Thin Solid Films* 420–421 (2002) 89.
- [43] C.F. Windisch Jr., G.J. Exarhos, K.F. Ferris, M.H. Engelhard, D.C. Stewart, *Thin Solid Films* 398–399 (2001) 45.
- [44] J. Bruneaux, H. Cachet, M. Froment, A. Massad, *Thin Solid Films* 197 (1991) 129.
- [45] Y. He, J. Zhang, X. Yang, Q. Xu, X. Liu, C. Zhu, X. Hou, *Microelect. J.* 36 (2005) 125.
- [46] N. Barsan, U. Weimar, *J. Electroceram.* 7 (2001) 143.
- [47] S. Mishra, C. Ghanshyama, N. Rama, R.P. Bajpai, R.K. Bedi, *Sens. Actuators B* 97 (2004) 387.